PHYSICAL REVIEW E **66**, 066208 (2002)

# Excitable media in open and closed chaotic flows

Zoltán Neufeld,[1] Cristóbal López,[2] Emilio Hernández-García,[3] and Oreste Piro[3]
[1]*Department of Applied Mathematics and Theoretical Physics, University of Cambridge, Silver Street, Cambridge CB3 9EW, United Kingdom*
[2]*Dipartimento di Fisica, Università di Roma "La Sapienza," Piazzale Aldo Moro 2, I-00185 Roma, Italy*
[3]*IMEDEA (CSIC-UIB) Instituto Mediterráneo de Estudios Avanzados, Campus Universitat de les Illes Balears, E-07071 Palma de Mallorca, Spain*
(Received 4 September 2002; published 16 December 2002)

We investigate the response of an excitable medium to a localized perturbation in the presence of a two-dimensional smooth chaotic flow. Two distinct types of flows are numerically considered: *open* and *closed*. For both of them three distinct regimes are found, depending on the relative strengths of the stirring and the rate of the excitable reaction. In order to clarify and understand the role of the many competing mechanisms present, simplified models of the process are introduced. They are one-dimensional baker-map models for the flow and a one-dimensional approximation for the transverse profile of the filaments observed in the concentration patterns.

DOI: 10.1103/PhysRevE.66.066208 PACS number(s): 82.40.Bj, 82.40.Ck, 47.70.−n, 47.52.+j

## I. INTRODUCTION

Excitable media [1–3] are extended systems exhibiting a variety of pattern formation phenomena. They are often of chemical or biological nature, although they can also be found in other contexts [4,5]. Each spatial point in an excitable medium is described by a dynamical system in which *activator* and *inhibitor* variables can be identified. The *activator* displays some kind of autocatalytic growth behavior, but the presence of the *inhibitor* controls it so that the dynamical system has a stable fixed point as unique global attractor. The essence of the excitability phenomenon is the presence of a threshold, such that if the system is perturbed above it, the system variables reach the stable fixed point only after a large excursion in phase space. This behavior usually appears when the activator has a temporal response much faster than the inhibitor, which then takes some time before stopping the growth of the activator.

When different parts of a system are coupled diffusively, a local perturbation excites neighboring points, and as a result, the excitation propagates through the system as a wave (called *autowave* or *front*). This is a global phenomenon in the sense that all the points in the system will be reached by the wave and thus experience the excitation-deexcitation cycle, but is noncoherent, since only a small part of the system (the front) is excited at each time.

In many situations the excitable dynamics takes place in a fluid environment. One such example is the Belousov-Zhabotinsky reaction [6,7], intensively investigated in laboratory experiments. Another example is the population competition occurring in oceans or lakes between different plankton species: Truscott and Brindley [8] identified phytoplankton as the fast activator and zooplankton as the slow inhibitor in models of biological aquatic population dynamics. In such situations, different parts of the system interact not only via diffusion, but advective transport is present, and it can play also an important role [9]. One of the most obvious effects of stirring by the flow is that the concentrations would become more mixed and, for fast enough stirring, the whole extended system will behave homogeneously. Another effect, in this case present for slow stirring, is that the fronts would be deformed by the flow and eventually be broken [10]. A study covering the full range of stirring intensities was performed in Ref. [11], in the framework of flows leading to chaotic advection [12]. Among other results, it was shown that there is an intermediate range of stirring for which the whole system excites coherently.

In this paper we further analyze the situation addressed in Ref. [11], that is, excitable media under the effect of chaotic advection, and extend it by considering also stirring by open flows. As a striking result, we find situations in which excitation persists indefinitely in the system when stirred by an open flow, whereas the excitation process is a transient both under closed flows and in the absence of stirring. Additionally, a number of simplified one-dimensional models are introduced and used to gain insight and analytical predictions on the dynamical processes involved. We mention that studies in the same spirit than ours but for the different case of chemical reactions of autocatalytic or bistable type can be found in Ref. [13].

The paper is organized as follows: In Sec. II we present the basic framework and the chemical and two-dimensional flow models (closed and open) to be used. Section III describes numerical results for them. Section IV introduces one-dimensional simplified models that help to understand the above numerical results, and our conclusions are presented in Sec. V.

## II. REACTION-ADVECTION-DIFFUSION DYNAMICS

### A. General framework

Let us consider $N$ interacting species with concentrations $C_i(\mathbf{r},t)$, $i=1,2,\ldots,N$, transported by a flow $\mathbf{v}(\mathbf{r},t)$ that we assume incompressible. The governing reaction-advection-diffusion equations can be written as

$$\frac{\partial C_i}{\partial t}+\mathbf{v}\cdot\boldsymbol{\nabla}C_i=\mathcal{F}_i(C_1,\ldots,C_N;k_1,\ldots,k_M)+D_i\nabla^2C_i, \tag{1}$$

 

where the $\mathcal{F}_i(C_1,\ldots,C_N;k_1,\ldots,k_M)$ describe the interaction dynamics of excitable type among the components, and the parameters $k_i$ are the reaction rates. Although in some realizations of excitable reactions the diffusion coefficients can vary widely from one species to the other, as for example, when it takes place in a gel medium, in liquid media diffusion coefficients are rather similar and, for simplicity, we take in the following $D_i=D$, $\forall\ i$. It is convenient to adimensionalize Eq. (1) to have a clearer view of the processes involved. To this end, let us identify typical scale $L$ and speed $U$ of the flow. A typical time scale is thus $L/U$, and we perform the change of variables,

$$\mathbf{r}\to\mathbf{r}'\equiv\frac{\mathbf{r}}{L},\quad t\to t'\equiv\frac{tU}{L},\quad \mathbf{v}\to\mathbf{v}'\equiv\frac{\mathbf{v}}{U}. \tag{2}$$

We assume that the concentrations are already expressed in some convenient dimensionless units, so that the reaction rates have units of inverse time, and use one of the reaction rates, say $k_1\equiv k$, to define dimensionless reaction terms,

$$\mathcal{F}_i\to\mathcal{G}_i\left(C_1,\ldots,C_N;\frac{k_2}{k},\ldots,\frac{k_M}{k}\right)$$
$$\equiv k^{-1}\mathcal{F}_i(C_1,\ldots,C_N;k,k_2,\ldots,k_M). \tag{3}$$

With these changes, Eq. (1) reads

$$\frac{\partial C_i}{\partial t}+\mathbf{v}\cdot\boldsymbol{\nabla}C_i=\mathrm{Da}\,\mathcal{G}_i(C_1,\ldots,C_N;\epsilon_2,\ldots,\epsilon_M)+\frac{1}{\mathrm{Pe}}\nabla^2C_i, \tag{4}$$

where the primes have been omitted for notational simplicity. We have scaled the reaction rates in terms of the first one $\epsilon_i\equiv k_i/k$, $i=2,3,\ldots,M$, and

$$\mathrm{Da}\equiv\frac{kL}{U}\qquad\text{and}\qquad\mathrm{Pe}\equiv\frac{LU}{D} \tag{5}$$

are the Damköhler and the Péclet number, respectively. The Damköhler number measures the reaction speed in terms of the advection, whereas Pe is the ratio of advection to diffusion at scale $L$. The product Pe Da measures the importance of reaction with respect to diffusion. We will be interested in the regime of large Pe, so that diffusion is negligible except at scales much smaller than system size, and explore a range of values of Da. We consider several two-dimensional models of flow, and also one-dimensional simplifications of them. Sensible comparisons of the behavior under different flows would be facilitated by the introduction of the above adimensional framework, although perfect correspondence cannot be expected when they are not dynamically similar.

### B. Reaction and flow models

As a concrete example of reaction scheme of the excitable type, we focus on the FitzHugh-Nagumo (FN) model [1,2]. We note however that we expect all our qualitative results to apply to the general class of excitable systems. In fact, some early results for closed flows [11] have been already checked for models of plankton dynamics [14]. The FN model consists in a dynamics of the type (4) for two interacting species, of concentrations $C_1$ and $C_2$, and reaction terms,

$$\mathcal{G}_1=f(C_1)-C_2,\quad f(C_1)=C_1(a-C_1)(C_1-1), \tag{6}$$

$$\mathcal{G}_2=\epsilon(C_1-\gamma C_2), \tag{7}$$

where $\epsilon$ $(=\epsilon_2)$ is the ratio between the two time scales. The FN model shows excitable behavior when $\epsilon\ll 1$ so that there is a separation between the fast evolution of the active component $C_1$ and the slow evolution of $C_2$, the passive one or *inhibitor*.

In a homogeneous system, Eq. (4) becomes $\dot{C}_i=\mathrm{Da}\,\mathcal{G}_i$. When $C_2=0$, this dynamical system with Eq. (6) describes dynamics of a bistable reaction, so that initial conditions for $C_1$ below a threshold value $a$ decay towards the *unexcited* or *rest* state $C_1=0$, whereas initial conditions above $a$ evolve to the *excited* state $C_1=1$ in a time of the order of $\mathrm{Da}^{-1}$. But Eq. (7) implies that, as soon as $C_1$ grows above zero, the inhibitor $C_2$ grows also (on a time scale a factor $\epsilon$ slower) and as a result the excited state $C_1\approx 1$ is only a transient: in a time of the order of

$$\tau_e\approx C_2^M(\epsilon\,\mathrm{Da})^{-1}, \tag{8}$$

$C_2$ reaches $C_2^M$, which is the local maximum value of the function $f(C_1)$, and then deexcitation occurs. After a time of the order of $(\epsilon\,\mathrm{Da}\gamma)^{-1}$, during which the system cannot be excited (the *refractory* state) $C_1$ and $C_2$ return back to the fixed point or equilibrium value $C_1=C_2=0$. In the following we will use the values $\epsilon=10^{-3}$, $\gamma=3.0$, and $a=0.25$ for the parameters in the local FitzHugh-Nagumo dynamics. In this case, $C_2^M\approx 0.1$.

The flow is assumed to be imposed externally so that the chemical dynamics has no influence on the velocity field, $\mathbf{v}(\mathbf{r},t)$. We consider two different kinds of chaotic flows which, in other contexts, are known to behave rather differently: closed and open flows. In the first situation, fluid particles remain in a bounded region of space, and the flow produces mixing in the whole fluid. In the case of open flows, fluid particles enter the system and typically, after some time, they leave it. Interesting situations arise when, as an effect of the stirring, there are special orbits never leaving the system. For hyperbolic chaotic flows, such orbits form a fractal set of zero measure, the *chaotic saddle* [15] with stable and unstable manifolds. When a set of particles is released on that flow, most of them leave the system rapidly. But those on trajectories coming close to the stable manifold of the chaotic saddle become attracted by it and remain longer in the system. They finally escape the saddle, at a characteristic escape rate $\kappa$, tracing closely its unstable manifold.

As a simple two-dimensional and incompressible velocity field, we consider an archetype of closed chaotic flows, the motion generated by two alternating sinusoidal shear flows oriented along the $x$ and $y$ direction for the first and second half of a flow period $T$, respectively [16],

$$v_x(x,y,t)=\frac{A}{T}\Theta\left(\frac{T}{2}-t \bmod T\right)\sin\left(\frac{2\pi y}{L}+\phi_i\right),$$
$$v_y(x,y,t)=\frac{A}{T}\Theta\left(t \bmod T-\frac{T}{2}\right)\sin\left(\frac{2\pi x}{L}+\phi_{i+1}\right), \quad (9)$$

where $\Theta$ is the Heaviside step function. Note that all the geometric details of the stirring by the flow depend on the parameter $A$, while $T$ sets the speed of stirring without altering the trajectories of the fluid elements. In order to avoid Kolmogorov-Arnold-Moser (KAM) tori acting as transport barriers, typically present in time-periodic flows, the velocity field is made aperiodic by introducing a random phase $\phi_i$, which takes on independent values in each half period, and is uniformly distributed in the range $[0,2\pi]$. The fluid is confined in a square of lateral size $L$ with periodic boundary conditions, so that the flow is closed. $L$ and $T$ fix space and time scales for the flow, and $L/T$ is a typical velocity. Thus we can adimensionalize Eq. (1) in terms of these quantities, so that $\mathrm{Da}=kT$ and $\mathrm{Pe}=L^2(DT)^{-1}$. This leads to Eq. (4), written in units for which $L=T=1$. We set the remaining adimensional parameter $A/L=0.7$, for which the flow is nearly ergodic. The numerically computed Lyapunov exponent is $\mu\approx 1.66/T$.

As a simple example of open flow, we take a blinking vortex-sink system [17,18] consisting of two alternately opened point sinks in an unbounded two-dimensional domain. Around each sink, the velocity field is a combination of a point vortex and a point sink given by the complex potential

$$w(z)=-(Q+iK)\ln|z-z_s|. \quad (10)$$

$z_s$ gives the position of the sink in the complex plane $\{z,z\in\mathcal{C}\}$, so that $z-z_s=re^{i\phi}$ defines polar coordinates $(r,\phi)$ around the sink. The imaginary part of $w(z)$, $\Psi=-K\ln r-Q\phi$ is the stream function, from which the fluid particle equations of motion are

$$\dot{r}=\frac{1}{r}\frac{\partial\Psi}{\partial\phi}=-\frac{Q}{r},$$
$$r\dot{\phi}=-\frac{\partial\Psi}{\partial r}=\frac{K}{r}. \quad (11)$$

The fluid trajectories can be explicitly integrated,

$$r(t)=\sqrt{r_0^2-2Qt},$$
$$\phi(t)=\phi_0-\frac{K}{Q}\ln\frac{r(t)}{r_0}. \quad (12)$$

The fluid particles come from infinity following logarithmic spirals of circulation given by $2\pi K$. The flow is incompressible everywhere, except at the sink core $z_s$, where an area of fluid $2\pi Q$ disappears per unit of time (the trajectories in a circular region of this area around $z_s$ have their trajectories undefined after one time unit because of Eq. (12) and they should be understood to leave the system): we have thus an open flow. The motion is not chaotic if $z_s$ is a unique static point. The *blinking vortex-sink* flow consists in considering the active sink position to be at $z_s=(0,d)$ during half a period $T/2$, and at $z_s=(0,-d)$ during another half a period. This corresponds physically to opening and closing alternatively two sinks separated by a distance $2d$. Typical space, time, and velocity scales are $d$, $T$, and $d/T$, respectively. From them, $\mathrm{Da}=kT$, and $\mathrm{Pe}=d^2(DT)^{-1}$, and we can use Eq. (4) in the units in which $d=T=1$. The flow is fully characterized by the adimensional sink strength $\eta=QT/d^2$ and the ratio of vortex to sink strength $\xi=K/Q$. We take $\eta=1$ and $\xi=10$. For these parameter values, the Lyapunov exponent on the saddle and the escape rate from it are [18] $\mu=2.19/T$ and $\kappa=0.54/T$, respectively.

## III. NUMERICAL RESULTS

The numerical integration of the reaction-advection-diffusion problem has been carried out on a square grid of $1000\times 1000$ points, with grid size $\Delta x$, by using a simple semi-Lagrangian scheme for the transport processes combined with a fourth-order Runge-Kutta method for the time integration of the local chemical dynamics. The semi-Lagrangian advection step at time $t$ consists in calculating, from any gridpoint, a time-backwards Lagrangian trajectory for a time $\Delta t$. Then the concentrations at this fluid element are calculated by bilinear interpolation from the concentrations on the grid at time $t-\Delta t$, and these concentration values are then assigned to the starting gridpoint at time $t$. The interpolation step introduces an effective diffusion $D\approx(\Delta x)^2/\Delta t$, which limits the maximum Pe number we can attain. Since the numerical diffusion is not uniform in space, we also include an explicit diffusion step corresponding to the same Pe number.

Initially the system is in the homogeneous steady state, $C_1=C_2=0.0$, and then it is perturbed by a localized Gaussian pulse in the concentration of the *activator* component

$$C_1(x,y,t=0)=C_0\ \exp[-(x^2+y^2)/2l_0^2], \quad (13)$$

where $C_0$ is chosen to be larger than the excitation threshold $a=0.25$, and the size of the perturbation, $l_0$, is much smaller than the system size, $L=1$. The dependence of the results on the particular values of $C_0$ and $l_0$ will be discussed later. The inhibitor component $C_2$ is not perturbed initially. We study the response of the system for different values of the adimensional reaction rate Da, keeping the rest of the parameters fixed. In the absence of flow ($\mathrm{Da}=\infty$) the initial condition (13) produces a circular ring of excitation (a *target* wave; in fact the structure of the target wave is such that the excitation ring is followed by a refractory ring) that expands in radius until reaching the system boundaries. We will see that this behavior is strongly modified at finite Da.

### A. Closed flow

The model (9) is integrated numerically on the unit square, $L=1$, with periodic boundary conditions, from the initial condition described above. The resolution is thus $\Delta x=10^{-3}$. We use $\Delta t=10^{-3}$ (in units of the flow period) and thus $\mathrm{Pe}\approx 1000$.

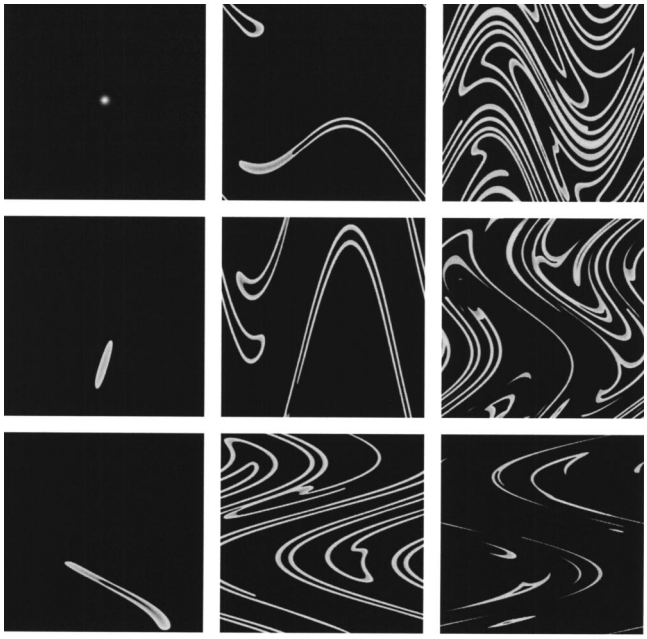

FIG. 1. Activator concentration at different times under stirring by the closed flow, for Da=300 and Pe≈1000. The initial condition had $C_0=0.5$ and $l_0=0.01$. The sequence runs from top to bottom, and then from left to right. The total time lapse is three periods of the flow. Dark and clear gray level indicates, respectively, low and high activator values. A noncoherent process of global excitation is seen.

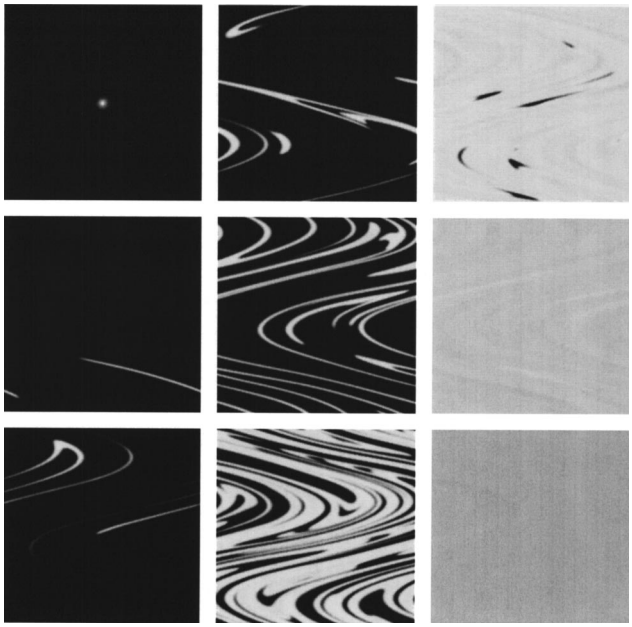

FIG. 2. Same as Fig. 1, but at Da=25. The interval between snapshots is of 1.2 time units. A process of coherent global excitation is seen. At longer times (not shown) the system returns homogeneously to the unexcited state.

Snapshots of the spatial structure for Da=300 and Da =25 are shown in Figs. 1 and 2, respectively. In the first case, the localized perturbation gives rise to an excited patch (with its interior in the refractory state) that is the stirred version of the circular wave front that would be produced in the absence of flow. The patch is elongated into a convoluted filamental structure by the chaotic flow and eventually visits all the points of the system. The filaments have a characteristic *double-line* structure with refractory area in the center. The excitation is global, in the sense that all the points of the system have become excited at some moment, but is not coherent, since only a part of the system is excited at a given moment, being the rest in the refractory or in the equilibrium state.

In a range of smaller Da numbers, a qualitatively different phenomenon occurs: The initial patch is again stretched into a growing filament, but now the filaments are thinner that prevents the formation of refractory region within them. This results in a coherent global excitation when the filaments fill up the whole system. Figure 2 is a representative example of this situation. Once fully excited, the system remains homogeneous and its subsequent decay to the unexcited state occurs everywhere at the same time. In this second part of the dynamics, mixing becomes irrelevant since there is nothing to mix in a homogeneous configuration.

At still smaller Da (faster stirring or slower chemistry), a sharp transition to a new dynamic regime occurs: below a critical Da number- $\mathrm{Da}_c$, the excitation dies without propagating significantly; dilution is fast and dominates over the growth rate of the activator. By *dilution* we mean the process of mixing of the excited patch with the surrounding unexcited fluid, leading to the decreasing and elimination of excitation in the patch. This mixing is originated by the diffusive flux from inside the patch (high value of the activator) to outside (low activator value). The value of $\mathrm{Da}_c$ depends only slightly on the details of the initial condition [as long as $C_0$ remains suprathreshold and $l_0$ much smaller than system size and above some diffusion-controlled minimum size, of the order of Eq. (22), discussed below]. For example, if $C_0=1$ and $l_0=0.1$, 0.05, and 0.02, one finds $\mathrm{Da}_c\approx 12.0$, 14.2, and 16.3, respectively.

Figures 3 and 4 summarize the different situations. Figure 3 shows the time dependence of $\langle C_1\rangle$, the space average of the concentration of $C_1$, and Fig. 4, the maximum value attained by $\langle C_1\rangle$. For increasing Da the coherence of the

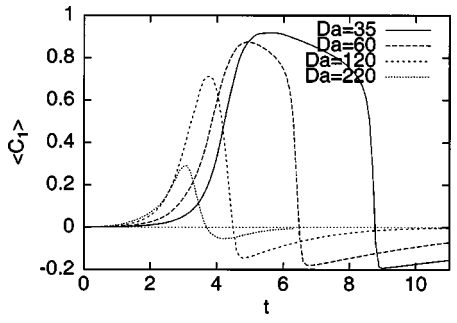


FIG. 3. Time evolution of the mean concentration at various values of Da. $C_0=0.5$ and $l_0=0.01$. Time is in units of $T$. By further decreasing Da, this time evolution changes suddenly, at $\mathrm{Da}_c$, to a fast decay of the initial condition that is indistinguishable, at the scale of this plot, from the horizontal axis at zero mean concentration.

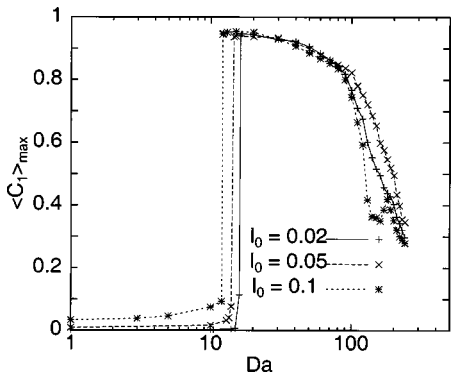


FIG. 4. The maximum value attained by $\langle C_1 \rangle$ as a function of Da. In all cases the initial condition had $C_0=1$, and $l_0$ was as indicated.

global excitation is gradually lost so that the maximum value of the average concentration is below the one corresponding to the fully excited state.

### B. Open flow

Since an infinite domain cannot be simulated easily in the computer, a square domain of size $L/d=6$ is considered instead. With a lateral discretization of 1000 points, this leads to $\Delta x=6\times10^{-3}$. We use $\Delta t=2\times10^{-3}$ (in units of the flow period) and thus Pe$\approx$56. Concentrations at the boundaries are kept at the fixed-point values $C_1=C_2=0$. The interior of the domain is initialized also in this state except for the perturbation in $C_1$, Eq. (13), located in the middle position between the two sinks.

For small Da, as in the closed flow case, the perturbation is diluted by the flow before significant wave propagation occurs, and the excited material soon leaves the system through one of the sinks. By increasing Da, a sharp transition to a new regime occurs: In response to the persistent arrival of unexcited reactants from the boundaries, and despite the continuous loss of fluid through the sink, a steady pattern of excitation is permanently sustained by the autocatalytic behavior of the activator. An example of the time evolution is shown in Fig. 5, and a snapshot in Fig. 6. The excited pattern closely traces a fattened version of the unstable manifold associated to the chaotic saddle of this open flow [18], and as this manifold, it fluctuates periodically in time. The value $\mathrm{Da}_c\approx14.5$ at which this transition occurs is in the range of the values obtained for the closed flow, thus suggesting that the mechanism for it is rather local and independent of the details of the flow.

The filaments in the excited pattern fatten up with increasing Da. Suddenly, a new regime is reached above a second critical Da$\approx$90.5: the excitation initially accumulates at the unstable manifold of the chaotic saddle, as before, but this is just a transient that is followed by an irregular recovery of the equilibrium ($C_1=C_2=0$) state everywhere. This new regime has some analogies with the large Da behavior under the closed flow, for which a noncoherent excitation occurred (and the transition value of Da is of the same order), but here it appears suddenly as a function of Da, and the excitation does not visit the full system but remains close to the unstable manifold of the chaotic saddle.

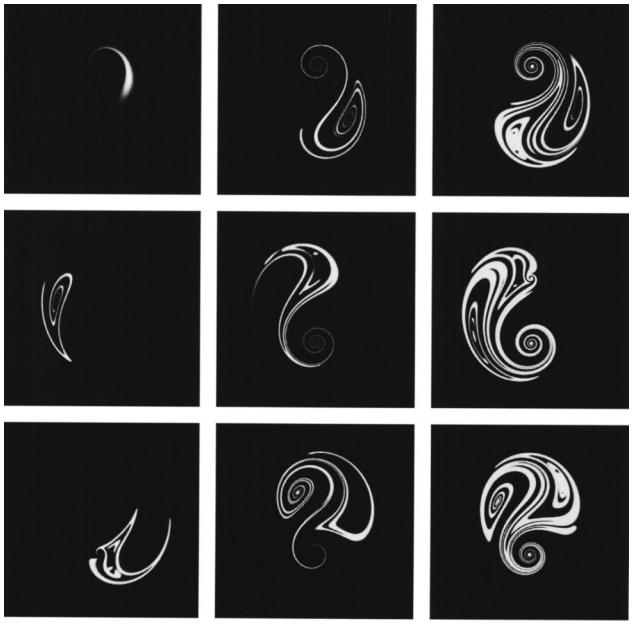

FIG. 5. Time evolution of the activator concentration under the open flow. The snapshots are shown every 0.7 time units, from top to bottom and then from left to right, starting 0.7 time units after the initial perturbation, Da=50 and Pe$\approx$56. After the last time shown, excitation is maintained indefinitely in the system, and the long-time pattern, which follows the shape of the unstable manifold of the chaotic saddle, repeats periodically in synchrony with the flow.

The whole behavior is summarized in Figs. 7 and 8, where the time evolution of the mean value of the activator, and its asymptotic long-time value (not the maximum value as in Fig. 4), is plotted versus Da. There is a range of Da in which a finite amount of excited fluid remains permanently in the system, despite the openness of the flow.

The existence of critical values of Da or equivalently of critical stirring rates can be seen to be a consequence of the competition between a number of processes. In the closed flow case, advection and diffusion tend to homogenize and dilute the excited patch, while the excitable dynamics in-

FIG. 6. Snapshot of the activator concentration maintained in the system at long times, for Da=20.

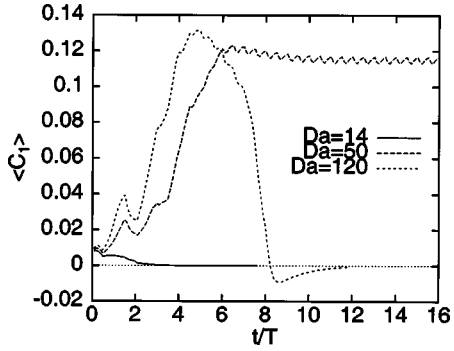


FIG. 7. Time evolution of the average concentration $\langle C_1 \rangle$ for three values of Da. $C_0=0.5$, $l_0=0.05$.

creases the local concentration of the active component wherever the excitation threshold is exceeded. In the open flow, there is an additional factor: the escape rate of fluid particles from the system. In order to gain further insight we attempt to separate the essential ingredients that contribute to the observed behavior, and consider reduced models of the problem.

## IV. REDUCED MODELS

### A. One-dimensional baker model for the closed flow

The main effect of chaotic advection is to stretch and fold fluid elements producing the filamentary patterns visible in the figures of the preceding section. Perhaps the simplest model of this is the so called *baker transformation*. Baker-map models have been used recently by Toroczkai *et al.* [19] to study autocatalytic reactions in open chaotic flows. A single action of the baker transformation on the unit square can be described as a stretching along the $y$ axis by a factor of 2, followed by compression by a factor of 2 along the $x$ axis. Then the resulting rectangle is cut into two pieces of unit length along the $y$ direction and placed back on the unit square. This model of chaotic advection neglects spatial nonuniformities of the stretching and curvature of the filaments, present in a general flow. Nevertheless, since it is a discrete-time map, it is strongly nonuniform in time.

If the initial perturbation is taken to be homogeneous in the $y$ direction this is preserved by the baker transformation and the problem becomes one dimensional. Even for arbitrary initial conditions the concentrations are rapidly homogenized along the $y$ direction by the repeated stretching, and after a short time the one-dimensional description becomes relevant. This may be regarded as a general feature of transport problems in the presence of stirring, since one can associate local stretching directions to any point of the flow and the problem can be reduced to the description of the filamental structure in the transverse direction. In the one-dimensional formulation the baker transformation $\mathcal{T}$ acts by replacing the concentration field by two copies compressed by a factor of 2 placed next to each other. To better represent the process of filament folding, the left half is not a copy but the mirror image of the right half.

$$\begin{aligned} &\mathcal{T}: \quad x \to \mathcal{T}x = x/2, (2-x)/2, \\ &C_i(x) \to \mathcal{T}C_i(x) = C_i(\mathcal{T}^{-1}x). \end{aligned} \tag{14}$$

Numerical simulations on the unit interval with periodic boundary conditions of the one-dimensional FitzHugh-Nagumo system with the baker transformation applied at discrete times ($t=nT, n=1,2,\ldots$), and diffusion and chemistry acting between them, show qualitatively similar regimes to the two-dimensional closed flow presented above, including the transition to global excitation that occurs in an intermediate range of $\mathrm{Da}=kT$.

Time evolutions of the activator spatial structure are shown in Fig. 9, for three different values of Da, and two of $\mathrm{Pe}=L^2/DT$. The excited regions can be interpreted as transverse cuts through filaments. The number of filaments is doubled by each action of the baker map, while the decreasing of their width may be, or may be not, compensated by the effect of excitable growth. When growth is slow (upper left panel in Fig. 9), the filaments become narrower until a point in which diffusive mixing with the surrounding unexcited fluid destroys them and excitation disappears. By increasing Da (upper right), the filament width reaches a minimum nonvanishing value with its central $C_1$ concentration value well above the threshold $a$. The effect of the baker map is here to join together a number of filaments until diffusion homogenizes the distribution. Since the homogenized value of $C_1$ is above the threshold, a coherent excitation follows. After some time the excitation disappears homogeneously and the system returns to the nonexcited state.

In the case of large Da (lower panels), the reaction is fast enough to approach the refractory state in the middle of the filaments before significant compression. The filaments thus acquire the double-hump structure that was also seen in the full two-dimensional simulation (Fig. 1). This fact works against the possibility of a coherent excitation, and there are two mechanisms by which the noncoherent excitation dies. At large enough Pe (lower left panel of Fig. 9), the excited parts of the filaments are narrow, and the periodic contraction produced by the baker map eventually brings them below a width such that the diffusion can eliminate them, in a way similar to what happens with the full filament at small Da (but here there is around abundant refractory material that helps the process). When Pe is decreased, the excited parts of the filaments travel faster, and collisions leading to filament

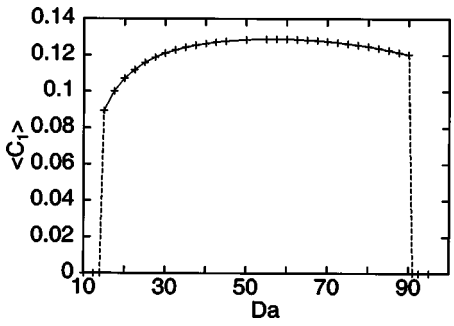


FIG. 8. Long-time asymptotic value of the average concentration $\langle C_1 \rangle$ as a function of Da. It is nonzero in a range of intermediate values.

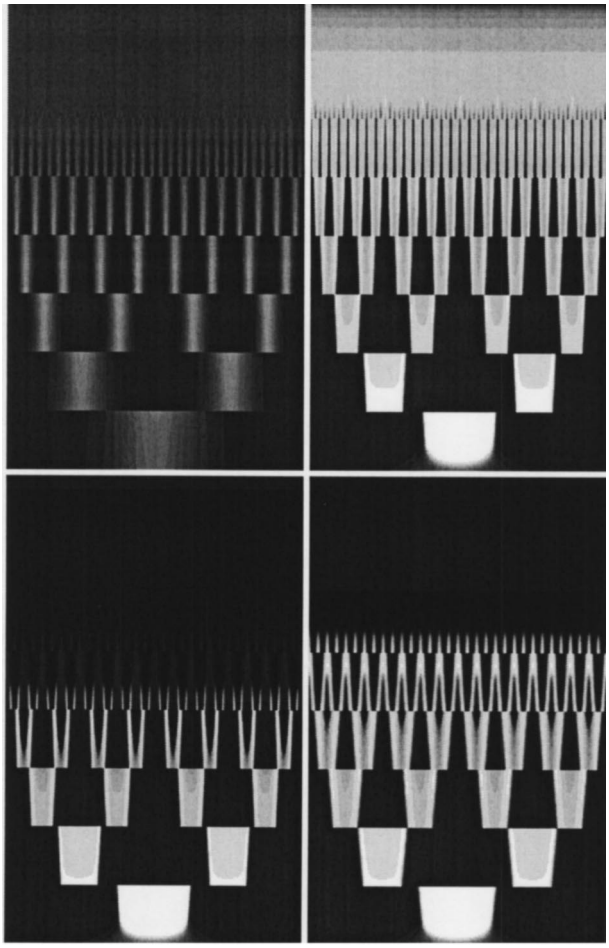

FIG. 9. Spatiotemporal evolution of $C_1$ for Da$=1$ and Pe $=1000$ (upper left), Da$=10$ and Pe$=1000$ (upper right), Da$=40$ and Pe$=1000$ (lower left), and Da$=50$, Pe$=400$ (lower right) under the baker model. Space is in the horizontal direction, and time runs in the vertical from bottom to top. Darker gray represents smaller values of $C_1$. The discontinuities appear at each application of the baker map, i.e., at times $T$, $2T$, $3T$, etc.

annihilation (because of the refractory material arriving after the excited filament) are the main mechanism killing the excitation (lower right panel of Fig. 9).

The phenomenology found here is fully consistent with the numerical simulations of Sec. III. But now, in addition to having a much simpler numerics, the mechanisms are easier to identify. Thus, stretching and folding, the characteristics implemented in the baker map, are enough to understand the effects of chaotic advection on excitable advection-reaction system. We stress, however, that the Da values at which the different transitions occur are of the same order, but not identical, to the ones found in the two-dimensional models. This was expected since there is no complete dynamical similarity between the present baker model and the flow models of Sec. III.

In the baker-map model the spatial structure is, by construction, periodic with period $L/n, n=[t/T]$. Thus the evolution of the system can be fully described by solving the same problem on an interval compressed by a factor of 2 at times $t=nT$ with periodic boundary conditions. This suggests, in general, that the evolution of the system can be captured by focusing on the transverse profile of a single filament subject to a typical stretching, and taking into account the decreasing separation between the filaments by appropriate boundary conditions. In fact, the main mechanism controlling the final homogenized value is the competition between the compression by the flow, and the tendency to expansion due to reaction diffusion. This mechanism is better analyzed by considering an isolated single filament, as will be done in Sec. IV C.

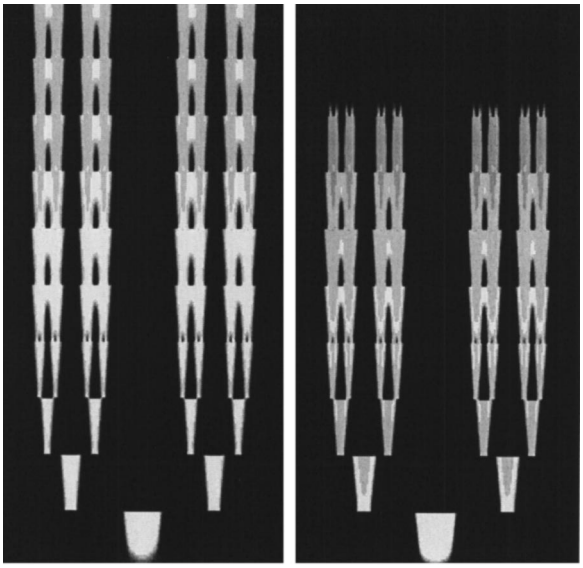

FIG. 10. Concentration of $C_1$ under the open baker map for Da$=30$ (left) and Da$=50$ (right). Space is in the horizontal direction, and time in the vertical, running from bottom to top. Darker gray levels correspond to lower values of $C_1$. Pe$=10^4$.

### B. One-dimensional baker model for the open flow

As in the closed flow case, we can implement the essentials of chaotic advection in open flows: stretching, folding, and escape, by a one-dimensional version of the open baker map. At times $nT$, $n=1,2,\ldots$, the unit interval ($L=1$) is compressed a factor of 3; two copies of the resulting compressed configuration are placed back into the initial square (one of them with orientation reversed) and the remaining third is filled with unexcited material ($C_1=C_2=0$). This represents the loss of one third of the fluid per map step, and its substitution by fresh reactants. Standard diffusion with periodic boundary conditions, and FitzHugh-Nagumo dynamics act between successive applications of the map.

The phenomenology observed is again qualitatively consistent with the two-dimensional simulations. For small Da the initial excitation is diluted before significant propagation. At larger Da (Fig. 10, left panel), the excitation approaches the chaotic saddle of this map, which is a standard Cantor set, and covers it with a finite width. A dynamic equilibrium is reached between filament merging and filament replication, so that the excitation is maintained indefinitely in the system. Increasing further Da leads to a second transition to a situation in which the excitation finally disappears, in much

the same way as in the closed flow. Again this happens when the filaments begin to develop the refractory state in its interior, and it may occur by two mechanisms: the one shown in the right panel of Fig. 10 which involves complex filament interaction, or simply the repeated contraction of the narrow excited parts at both sides of the refractory center. This last mechanism dominates at very large Pe.

Both in the open and in the closed flow case, the mechanisms leading to transitions and qualitative changes in the excitation behavior seem to be linked to properties of individual filaments, namely, the existence of a minimum width below which the filament disappears, and the development of a double-hump shape by increasing Da. Both phenomena can be understood to great detail by focusing on the behavior of an isolated filament.

### C. A one-dimensional filament model

We can address the analysis of the one-filament problem by replacing the flow by a time-continuous stretching in a pure strain flow, $v_x=-\lambda x$, $v_y=\lambda y$. This has in common with chaotic advection and with the baker map the local contraction and expansion along special directions, although it misses completely the folding behavior that leads to filament interaction at long times. According to the discussion above the relevant dynamics is along the convergent direction ($x$) of the flow. Thus, we propose that the evolution of concentrations $C_i(x,t)$ in a chaotically advected excitable medium can be described locally by

$$\frac{\partial}{\partial t}C_i-\lambda x\frac{\partial}{\partial x}C_i=\mathcal{F}_i(C_1,\ldots,C_N)+D\frac{\partial}{\partial x^2}C_i, \quad (15)$$

where $\lambda$ is the strain due to the flow [20,11,13]. In general, the strength and direction of the stretching fluctuate in space and time. Thus a suitable prescription for fixing a unique $\lambda$ should be established. This issue will be discussed later. A way to take into account multifilament situations in the framework of Eq. (15), is to impose periodic boundary conditions on an exponentially shrinking interval of length $L=\exp(-\lambda t)$, taking into account the decreasing interfilamental distance. But we will consider here the case of an isolated filament in a large (ideally infinite) one-dimensional domain.

We note that the one-dimensional model (15) does not conserve the amount of fluid on the line. This is more clearly seen by rewriting it as

$$\frac{\partial}{\partial t}C_i+\frac{\partial}{\partial x}\left(-\lambda xC_i-D\frac{\partial}{\partial x}C_i\right)=\mathcal{F}_i(C_1,\ldots,C_N)-\lambda C_i. \quad (16)$$

Whereas the left hand side is clearly written in a flux-conservative form, the term $-\lambda C_i$ in the right hand side represents fluid escape from the line at a rate $\lambda$. The reason for that is that Eq. (15) comes from a strain flow in which there is motion along the $y$ axis, and the term $\lambda C_i$ is simply the flux in that direction for concentrations homogeneous along $y$: $\lambda C_i(x)=\partial_y[\lambda y C_i(x)]$.

The pure strain flow has a time scale, $\lambda^{-1}$, that can be used to adimensionalize times, but there is no typical length scale. However, we can measure lengths in units of the diffusion length $\sqrt{D/\lambda}$ and then Eq. (15) becomes

$$\frac{\partial}{\partial \bar{t}}C_i-\bar{x}\frac{\partial}{\partial \bar{x}}C_i=\widetilde{\mathrm{Da}}\;\mathcal{G}_i(C_1,\ldots,C_N)+\frac{\partial^2}{\partial \bar{x}^2}C_i, \quad (17)$$

with $\widetilde{\mathrm{Da}}=k/\lambda$, $\bar{t}=\lambda t$, and $\bar{x}=x(D/\lambda)^{-1/2}$. Thus, we can always set $\mathrm{Pe}=L^2\lambda/D=1$ by choosing the units of $L$ or, in other words, the only effect of variations of diffusion strength in this model is a change in spatial scale. Qualitative changes can only occur by varying $\widetilde{\mathrm{Da}}$, that is, by changing $k$ or $\lambda$. This is clearly a limitation of the model and tells us that it can only be trusted in regions where there are well separated filaments of size much smaller than characteristic spatial scales of the velocity field (which are neglected when assuming a pure strain). We expect this to be a reasonable global approximation at sufficiently large Pe. Other phenomena neglected by this one-dimensional model are strain inhomogeneities and departure from one dimensionality.

In this section we mainly present our results in terms of the parameter $\widetilde{\mathrm{Da}}$ of Eq. (17), but eventually we would need to return to the units of Eq. (15), where the individual processes and scales are more easily identified. In the search of clarity, quantities representing lengths will be marked with an overbar when measured in the units of Eq. (17), that is, in units of the diffusion length. We also note that changing the strain $\lambda$ in Eq. (15) changes $\widetilde{\mathrm{Da}}=k/\lambda$ and also the units of space and time in Eq. (17).

Numerical solution of Eq. (17) for $\widetilde{\mathrm{Da}}$ not too small reveals that its long-time attractors are steady pulses of excitation concentrated near the origin. They can be interpreted as transverse cuts of the filaments observed in the two-dimensional models. Examples are shown in Figs. 11(a) and 11(b), where we plot the $C_1$ and $C_2$ concentration fields, respectively, for different values of $\widetilde{\mathrm{Da}}$ (the insets will be discussed below). The steady finite width of the filaments arises from compensation between the contracting tendency of the strain and the expanding tendency of the combined effect of diffusion and reaction. A simple quantitative argument [11] formalizing this consists in identifying the equilibrium half-width of the filament solutions of Eq. (15), $w_s$, as the distance to the center at which the strain speed $\lambda w_s$ exactly compensates the speed the front would have in the absence of strain, $v_f$. Since this velocity may be calculated for small $\epsilon$ [2]: $v_f=(1-2a)\sqrt{Dk/2}$, $w_s$ is obtained from $\lambda w_s=v_f$. In the adimensional space units and parameters of Eq. (17) it reads

$$\bar{w}_s=(1-2a)\left(\frac{\widetilde{\mathrm{Da}}}{2}\right)^{1/2}. \quad (18)$$

The existence, for $\widetilde{\mathrm{Da}}$ above (or $\lambda$ below) a given value, of these steady filaments with finite width provides an explanation for most of the phenomenology discussed in the previous sections. In two-dimensional situations, the filament

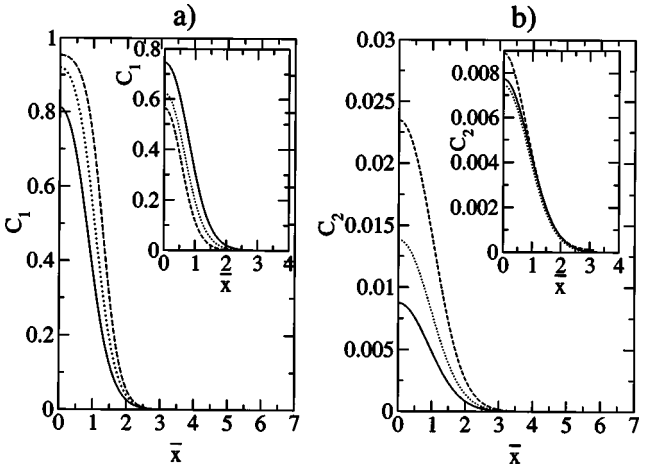


FIG. 11. (a) $C_1$ profiles for stable one-humped solutions of Eq. (17). In the inset the corresponding unstable solutions. Solid line is for $\widetilde{\mathrm{Da}}=12.99$, close to the disappearance of the filament solution, dotted line for $\widetilde{\mathrm{Da}}=16.77$ and dashed line for $\widetilde{\mathrm{Da}}=25$. (b) The same as (a) but for the $C_2$ concentration field. All the curves are symmetric with respect to $\bar{x}=0$, so that only positive $\bar{x}$ values are plotted.

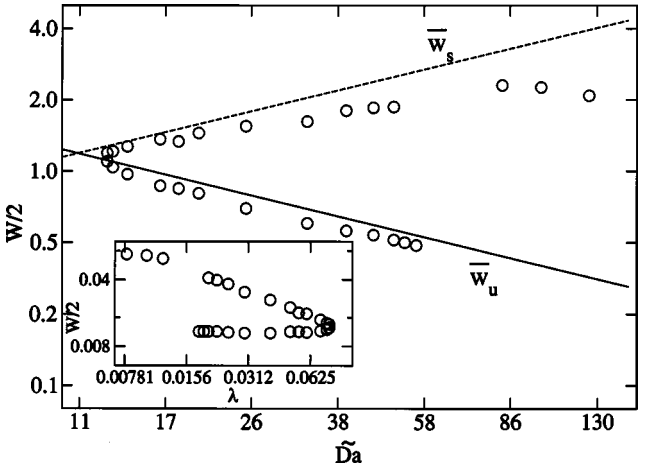


FIG. 12. Half-widths measured at the level of the excitation threshold ($C_1=0.25$) for the $C_1$ stable and unstable filament solutions of Eq. (17) in terms of $\widetilde{\mathrm{Da}}$ (log-log scale). Circles show the numerical values and the lines the analytical curves: solid line from Eq. (22) and dashed-line from Eq. (18). The inset shows the same numerical widths but in the dimensional units of Eq. (15) (we use $k=1$ and $D=10^{-5}$) as a function of λ, to stress the insensitivity of the width of the lower (unstable) branch to the strain λ.

will maintain its transverse shape while it expands in the longitudinal direction. After repeated folding, it will cover the whole system in the closed flow case, or cover the unstable manifold of the chaotic saddle in the open flow case. What will happen later will depend on the interactions between different parts of the excited filament, or on its response to strain fluctuations.

We observe that the steady-filament stable solution disappears for $\widetilde{\mathrm{Da}}<\widetilde{\mathrm{Da}}_c\approx 12.5$. This provides an explanation for the absence of excitation in the two-dimensional simulations below a critical Da: as far as the results of the one-dimensional model can be extrapolated there, a growing filament state cannot be reached at small Da because a steady (nondecaying) solution of the filament profile does not exist. To better understand the disappearance of the filament solution, we note that, in addition to the direct numerical simulation, an alternative way of finding the steady filaments is to solve by a shooting method [21] the steady state version of Eq. (17) which is obtained by setting $\partial_{\bar{t}} C_i=0$. With this method one can obtain all the steady solutions, not only those that are dynamically stable. It turns out that, in addition to the excited filament [and to the trivial homogeneous solution $C_1(\bar{x})=C_2(\bar{x})=0$], there is another pulse solution which is dynamically unstable. This unstable solution is shown, for several values of $\widetilde{\mathrm{Da}}$, in the insets of Fig. 11. It contains a marginal amount of excitation, in the sense that initial conditions with slightly less excited material evolve towards the stable homogeneous state, and initial conditions slightly more excited lead to the stable excited filament. It represents the unstable point in function space at which the activator growth exactly compensates the diffusive flux towards the exterior. In Fig. 12 we plot the width of the stable and unstable steady-filament solutions of Eq. (17). Here it is clear that the disappearance of the stable filament arises from collision with the unstable pulse in a saddle-node bifurcation.

Physically, increasing strain reduces the width of the stable filament, so that it approaches the unstable one, which is the limit below which excitation decays. The saddle-node bifurcation will occur when both widths are equal.

Since the width of the unstable pulse around $\bar{x}=0$ is rather small, we expect strain effects to be of minor importance in determining its shape, at least when $\widetilde{\mathrm{Da}}$ is not too close to $\widetilde{\mathrm{Da}}_c$. This is confirmed by the inset in Fig. 12, and also in the inset of Fig. 13 (to be discussed later). Hence, we can analytically estimate the shape of the unstable pulse and $\widetilde{\mathrm{Da}}_c$ in the following way: Since the amount of inhibitor is small everywhere for this solution [see the inset in Fig. 11(b)], and since we are interested in the situation $\epsilon\to 0$, we can approximate Eq. (15) (for $\lambda\approx 0$) by

$$kC_1(a-C_1)(C_1-1)+D\frac{\partial^2}{\partial x^2}C_1=0. \tag{19}$$

The unstable pulse $C_1^u(x)$ is the solution homoclinic to $C_1=0$. After multiplication of Eq. (19) by $\partial_x C_1(x)$, integrations with respect to $x$, and application of the proper boundary conditions, one finds [22]

$$C_1^u(x)=C_+-\frac{C_+-C_-}{1-\frac{C_-}{C_+}\tanh^2\left(\frac{x}{w_u}\right)} \tag{20}$$

with

$$C_\pm=\frac{2}{3}(1+a)\pm\left[\frac{4}{9}(1+a)^2-2a\right]^{1/2}. \tag{21}$$

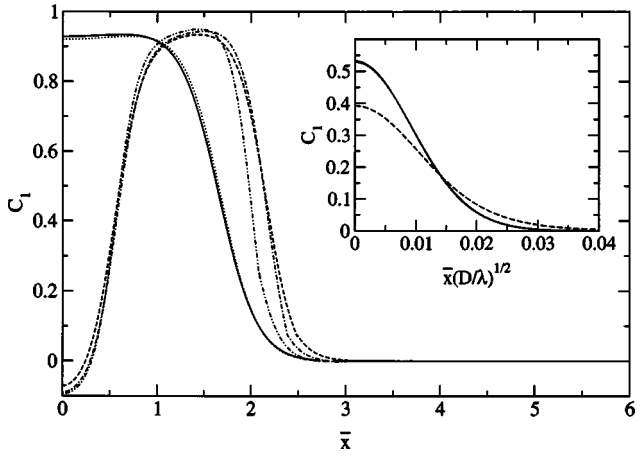


FIG. 13. Two-humped filament solutions for the $C_1$ field. Solid-line is for $\widetilde{\mathrm{Da}}=45.45$, when the two humps begin to develop. Dotted line $\widetilde{\mathrm{Da}}=50$, dashed line $\widetilde{\mathrm{Da}}=83.33$, dashed-dotted line $\widetilde{\mathrm{Da}}=100$ and dashed-double-dotted line for $\widetilde{\mathrm{Da}}=125$. In the inset we show the unstable solutions, for $\widetilde{\mathrm{Da}}=45.45$, 50, 52.63, and 55.55. In the scale of the plot, all of them collapse into the same solid-line curve, when plotted in terms of the physical space units of Eq. (15), as done here (we use $k=1$ and $D=10^{-5}$). The dashed line corresponds to the analytical solution given by Eq. (20).

$C_-$ is the maximum concentration at the center of the pulse, and its half-width is given by $w_u=2\sqrt{D/(ak)}$, or in the adimensional units of Eq. (17),

$$\overline{w_u}=\frac{2}{\sqrt{a\,\widetilde{\mathrm{Da}}}}. \tag{22}$$

In the inset of Fig. 13 we compare the analytical curve from Eq. (20) with the numerical values. We see that they are similar but not identical. We have checked that the reason for the discrepancy is the finite value of $\epsilon$ ($\epsilon=10^{-3}$). We have also performed calculations with smaller values of $\epsilon$ and seen that for the values of $\widetilde{\mathrm{Da}}$ in the figure, the approximate analytical solution (20) and the numerical one become virtually identical when $\epsilon\lesssim 10^{-5}$.

In any case, since the widths of analytical and numerical unstable pulses are very similar, we can estimate $\widetilde{\mathrm{Da}}_c$ by equating the above expressions (18) and (22) found for them: $\overline{w_s}=\overline{w_u}$, with the result

$$\widetilde{\mathrm{Da}}_c=\frac{2\sqrt{2}}{(1-2a)\sqrt{a}}. \tag{23}$$

For $a=0.25$ this gives $\widetilde{\mathrm{Da}}_c\approx 11.31$, that compares well with the numerically obtained value $\widetilde{\mathrm{Da}}_c\approx 12.5$ (see Fig. 12).

The saddle-node disappearance of the filament solutions in this one-dimensional filament model clearly gives an explanation for the sudden disappearance of excitation propagation at small Da in the two-dimensional models discussed in Sec. III, and in bakerlike models. To make the connection more quantitative, within the uncertainty given by the observed weak dependence of $\mathrm{Da}_c$ on characteristics of the initial perturbation (Fig. 4), one needs to identify the *effective* strain $\lambda$ in Eq. (15). If one identifies $\lambda\approx T^{-1}$, which is a reasonable measure of the strain in the models of Sec. III, then one has $\mathrm{Da}=\widetilde{\mathrm{Da}}$ and finds good quantitative agreement between the critical values of the Damköhler number for the filament model and the full two-dimensional simulations both in the open and in the closed flow case. But it should be said that, since the filaments are being advected by the flow, a more consistent choice for $\lambda$ would be the Lagrangian mean strain, given by the Lyapunov exponent $\mu$ of the advection dynamics. In the open flow case, the Lyapunov exponent on the chaotic saddle would be the analogous choice. These elections have been shown to be quantitatively successful in other situations [13]. With the values of $\mu$ stated in Sec. II B, this leads to $\mathrm{Da}=1.66\widetilde{\mathrm{Da}}$ for the closed flow and $\mathrm{Da}=2.19\widetilde{\mathrm{Da}}$ in the open case. Now the agreement has deteriorated. The effect of strain inhomogeneities may be rather important when the filaments are wide and have some diffusive motion, since then they can feel effective strains different from the Lagrangian one corresponding to a fluid particle at its center. Other effects related to the reduced dimensionality are also at play, since quantitative departures from the two-dimensional simulations appear already for the bakerlike models of Secs. IV A and IV B. Thus, one concludes that the one-dimensional filament model needs to be improved to provide systematic quantitative predictions on the behavior of reacting systems, but it does a very good job in identifying the basic mechanisms and qualitatively modeling them.

Still remaining to be discussed within the framework of this section are the qualitative changes of behavior occurring in the two-dimensional simulations at large Da: the progressive loss of coherence in the closed flow case, and the sudden disappearance of the persistent pattern in the open flow case. These phenomena were more or less coincident with the appearance of a double-hump structure in the filaments. Figure 13 shows that indeed the stable filament solutions of the one-dimensional model (17) begin to develop a double-humped structure for $\widetilde{\mathrm{Da}}\gtrsim 45$. A well developed double-humped shape establishes suddenly at $\widetilde{\mathrm{Da}}\approx 75.09$. One can understand this by noticing that the front solutions of Eq. (15) for $\lambda\approx 0$ have a finite width limited by the time during which excitation persists in the fluid particles (8), i.e., $\tau_e=C_2^M(\epsilon\widetilde{\mathrm{Da}})^{-1}$, in units of $\lambda^{-1}$. The width of the front is given in first approximation by $w_f\approx v_f\tau_e$. Interaction with the back of the front changes $C_2^M$ to a smaller value $C_2^J$, which is the solution of an algebraic equation [2]. For $a=0.25$, $C_2^J\approx 0.067$. It is reasonable to expect that when the total width of the filament, $2w_s$, exceeds twice the width of the front, $2w_f$, the filament will become unexcited in the middle. This argument would need corrections by the strain influence on $w_f$ and by the fact that the strain velocity in the middle of the filament is smaller than in the front (this would imply a shorter time of excitation, or smaller $C_2^J$). But in any case, this simple argument gives for the transition to two-

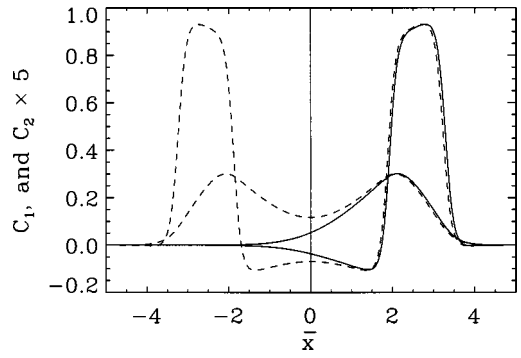


FIG. 14. Solid line is an asymmetric steady solution of Eq. (17) for $\widetilde{\mathrm{Da}}=200$. The higher curve is $C_1$ and the lower one $C_2$, multiplied by a factor of 5 to be visible in this scale. The dashed lines are symmetric solutions similar to the ones in Fig. 13, for $\widetilde{\mathrm{Da}}=200$ (upper curve, $C_1$, lower curve, $C_2$ multiplied by 5). Numerically we find that both solutions are simultaneously stable, each with its own basin of attraction.

humped filaments the condition $w_s \approx w_f$, that is, $\widetilde{\mathrm{Da}} \approx C_2^J \epsilon^{-1} \approx 67$, to be compared with the actual numerical value $\widetilde{\mathrm{Da}} \approx 75.09$.

We mention that the transition from the unimodal steady solution to the two-humped steady solution in the range $50 \lesssim \widetilde{\mathrm{Da}} \lesssim 70$ is associated with a complex bifurcation scenario in which different stable solutions coexist. For $\widetilde{\mathrm{Da}} \gtrsim 70$, additional asymmetric steady stable solutions to Eq. (17) appear. These are similar to the pulse solutions obtained without strain, but stopped by the flow. They have an excited head and a refractory tail. An example is shown in Fig. 14. The symmetric two-humped filaments found before, which remain linearly stable, can be thought as bound states of the two asymmetric ones.

The simple model studied in this section has allowed us to qualitatively understand the individual filaments seen in the full two-dimensional simulations, and in the baker model, to a great detail. What is completely missed here is the interaction between different filaments, or parts of the same filament. We have studied filament collisions in the context of Eq. (17) by initializing it with different combinations of displaced filament solutions. The analogy with the collisions in the models of the previous sections is far from complete, since here all the filaments evolve in the same simple velocity field $-\lambda x$, whereas in real multifilament situations, each filament has been created around its own local strain. Nevertheless, we have observed that collision between symmetric one-humped filaments leaves at long times a single centered one-humped filament, and collisions between two-humped filaments annihilate half of the humps, leading again to a single two-humped filament as the final state. The asymmetric frontlike filaments annihilate when colliding front to front, and bind in a two-humped filament when colliding tail to tail.

These observations help to understand the dynamic process of filament merging that leads to the persistent patterns in the open flows at intermediate Da. With the consideration of periodic boundary conditions, it is not difficult to understand also the process ending excitation in the closed flow at not too large Pe in terms of the annihilation of halves of two-humped filaments.

What seems to escape from the picture is the process ending the persistent pattern in the open flows at large Da: because of the openness of the flow, there are always filaments that do not collide with others, but that receive the fresh reactants entering the system. In this case, as in the situations of very large Pe, it seems that strain fluctuations are essential to understand the process of deexcitation. We have run model (15) with $\lambda$ randomly changing in time and found that, for large enough fluctuations, nonvanishing correlation time, and values of Da in the two-hump regime: the induced width fluctuations eventually end with the decay of the filament, in very much the same way as seen in the baker models simulations. We speculate that the larger width fluctuations originated by filament collisions in situations such as those in Fig. 10 (right panel) would amplify still more the effect of unsteady strain and help to eliminate excitation. Strain fluctuations in the baker model (periodic application of contraction followed by periods without strain) are an artifact of the discrete nature of the model. But in the two-dimensional simulations of Sec. III, and in real flows, strain fluctuations occur naturally and may be thus responsible for the excitation decay in the open flow at large Da. It is quite natural that this decay process only appears after the filaments develop the two-hump structure, since this implies the presence of refractory material. Nevertheless, a quantitative description of this process is still missing.

## V. CONCLUSIONS

We have analyzed the behavior of an excitable medium in the presence of open or closed chaotic flows. In both cases, three different regimes have been elucidated. The one at smaller Da, that is, the dilution of the excitation at fast stirring, is analogous to what is found in the case of bistable chemical dynamics [13].

The most interesting regimes are found at intermediate Da: in the closed flow case, a coherent excitation of the whole system arises from the localized perturbation, whereas in the open flow the excitation remains indefinitely in the system. This last phenomenon was also found under bistable and in autocatalytic dynamics [13], as well as the excitation phase under the closed flow, that is, the growth of an excited filament that becomes space filling. What is distinct of the excitable dynamics is that excitation under the closed flow is a transient, so that the system finally recovers the rest state, at variance with the bistable and autocatalytic behavior. It is striking that this recovery does not occur under the open flow in this intermediate Da range.

Also a consequence of the recovery behavior that characterizes the excitable dynamics, and that distinguishes it from the otherwise rather similar bistable dynamics, is the loss of coherence occurring at large Da. It manifests gradually under the closed flow, but as a sudden disappearance of permanent excitation in the open case.

A great part of our work has been devoted to the development of simplified models that help to understand the

above regimes and the transitions among them. Despite the strong approximations performed, these simple models reproduce, at least qualitatively, the full two-dimensional numerical results. The first simplified model is based in the use of a baker map for the advection dynamics. It highlights the processes of stretching and folding as the basic flow mechanisms leading to the aforementioned chemical regimes. The baker model dynamics also suggest that transitions are linked to the properties of individual filaments. Thus, an even simpler model is considered, where the stationary transverse profile of a filament is the main quantity under study. Most of the numerical observations can be understood within this framework, although some phenomena, specially those for which filament interactions seem relevant, would need of more detailed modeling.

Some geophysical observations have been already interpreted within the present framework [14]. It would be of great interest to perform experiments of chemical dynamics under well-controlled stirring to observe the different scenarios predicted here.

## ACKNOWLEDGMENTS

C.L. acknowledges financial support from the Spanish MECD. E.H.-G. acknowledges support from MCyT (Spain), Project Nos. BFM2000-1108 (CONOCE) and REN2001-0802-C02-01/MAR (IMAGEN).

[1] E. Meron, Phys. Rep. **218**, 1 (1992).
[2] J.D. Murray, *Mathematical Biology* (Springer, New York, 1993).
[3] M. Markus and B. Hess, Nature (London) **347**, 56 (1990); M. Markus, G. Kloss, and I. Kusch, *ibid.* **371**, 402 (1994).
[4] J.H.E. Cartwright, E. Hernández-García, and O. Piro, Phys. Rev. Lett. **79**, 527 (1997).
[5] M. Giudici, C. Green, G. Giacomelli, U. Nespolo, and J.R. Tredicce, Phys. Rev. E **55**, 6414 (1997).
[6] S.K. Scott, *Chemical Chaos* (Oxford University Press, Oxford, London, 1991).
[7] *Chemical Waves and Patterns*, edited by R. Kapral and K. Showalter (Kluwer Academic, Dordrecht, 1993).
[8] J.E. Truscott and J. Brindley, Bull. Math. Biol. **56**, 981 (1994); Philos. Trans. R. Soc. London, Ser. A **347**, 703 (1994).
[9] I.R. Epstein, Nature (London) **374**, 321 (1995).
[10] V.N. Biktashev, A.V. Holden, M.A. Tsyganov, J. Brindley, and N.A. Hill, Phys. Rev. Lett. **81**, 2815 (1998); V.N. Biktashev, I.V. Biktasheva, A.V. Holden, M.A. Tsyganov, J. Brindley, and N.A. Hill, Phys. Rev. E **60**, 1897 (1999).
[11] Z. Neufeld, Phys. Rev. Lett. **87**, 108301 (2001).
[12] H. Aref, Phys. Fluids **14**, 1315 (2002).
[13] Z. Neufeld, P.H. Haynes, and T. Tél, Chaos **12**, 426 (2002).
[14] Z. Neufeld, P.H. Haynes, V.G. Garçon, and J. Sudre, Geophys. Res. Lett. **29**, 1029 (2002).
[15] E. Ziemniak, C. Jung, and T. Tél, Physica D **76**, 123 (1994); J.C. Sommerer, H.C. Ku, and H.E. Gilreath, Phys. Rev. Lett. **77**, 5055 (1996).
[16] F. Városi, T.M. Antonsen, and E. Ott, Phys. Fluids A **3**, 1017 (1991); R.T. Pierrehumbert, Chaos, Solitons Fractals **4**, 1091 (1994).
[17] H. Aref, S.W. Jones, S. Mofina, and I. Zawadski, Physica D **37**, 423 (1989).
[18] G. Károlyi and T. Tél, Phys. Rep. **290**, 125 (1997).
[19] Z. Toroczkai, G. Károlyi, Á. Péntek, T. Tél, and I. Sheuring, J. Phys. A: Math Gen **34**, 5215 (2001).
[20] A.P. Martin, J. Plankton Res. **22**, 597 (2000).
[21] W. Press, S. Teukolsky, W. Vetterling, and B. Flannery, *Numerical Recipes in Fortran* (Cambridge University Press, Cambridge, England, 1992).
[22] M. Sanati and A. Saxena, Physica D **123**, 368 (1998).